Published in Journal of Sedimentary Research 72, issue 2, 252-267, 2002,
which should be used for any reference to this work

CARBONACEOUS AND PHOSPHATE-RICH SEDIMENTS OF THE MIOCENE MONTEREY FORMATION AT EL CAPITAN STATE BEACH, CALIFORNIA, U.S.A.

CÉDRIC M. JOHN[1,2], KARL B. FÖLLMI[1], ERIC DE KAENEL[3], THIERRY ADATTE[1], PHILIPP STEINMANN[1], AND CHRISTOPHE BADERTSCHER[1]
[1] *Institut de Géologie, Université de Neuchâtel, CH-2007 Neuchâtel, Switzerland*
[2] *Institut für Geologie und Paläontologie, Universität Stuttgart, D-70174 Stuttgart, Germany*
[3] *DeKaenel Paleo-Research, CH-2000 Neuchâtel, Switzerland*
e-mail: karl.foellmi@unine.ch

ABSTRACT: **The organic- and phosphate-rich interval of the Monterey Formation at El Capitan State Beach (west of Santa Barbara, California, U.S.A.; late early to early late Miocene in age) is composed of a carbonaceous marl (TOC contents between 1.2 and 23.2 wt %) with intercalated phosphate-rich laminae, lenses, and layers. Subordinate lithologies include ash layers, dolomitized horizons, and siliceous beds. We distinguished five lithological units: (1) a gray marl unit lacking major phosphate accumulations (> 16.3 Ma; average TOC content 2% by weight; average sedimentation rate 75 m/My; average TOC accumulation rate 0.19 mg/cm^2/yr); (2) a black marl unit including light-colored phosphatic laminae, lenses, and discrete particles (16.3–14.5 Ma; average TOC content 7.5% by weight; average sedimentation rate 20 m/My; average TOC accumulation rate 0.19 mg/cm^2/yr); (3) a red marl unit including light-colored phosphatic laminae, lenses, and commonly reworked particles (14.5–12.7 Ma; average TOC content 15% by weight; average sedimentation rate 20 m/My (14.5–13.3 Ma) and 2 m/My (13.3–12.7 Ma), respectively; average TOC accumulation rate 0.39 mg/cm^2/yr (14.5–13.3 Ma) and 0.04 mg/cm^2/yr (13.3–12.7 Ma), respectively); (4) a unit of complex and condensed phosphatic beds, interbedded with red marl (12.7–10.8 Ma; average sedimentation rate 3 m/My); and (5) a black marl unit with intercalated phosphatic laminae and lenses (< 10.8 Ma; average sedimentation rate 9 m/My; average TOC accumulation rate 0.09 mg/cm^2/yr).**

Phosphogenesis and accumulation of phosphate were dynamic processes, which started with local phosphogenesis leading to the formation of phosphatized particles, as well as stratigraphically bound phosphogenesis leading to the formation of phosphate laminae and lenses. Phases of subsequent sediment reworking resulted in the concentration of phosphate particles in phosphate-rich layers, and repeated phases of sediment reworking and phosphogenesis ultimately resulted in the formation of the complex phosphate condensed horizons. Preservation of organic matter was favored by high productivity rates and by the development of dysaerobic bottom-water conditions. The dynamic sedimentary environment likely led to the formation of early diagenetic phosphatic lids (which may have sealed off subjacent organic-rich layers) as well as to the rapid deposition of entire layers in the form of mud flows, thereby eventually enhancing the potential of organic-matter preservation.

Our new age data suggest that at the El Capitan State Beach section the intervals characterized by high TOC values and maximum TOC accumulation rates (red marl), as well as significant quantities of *in situ* phosphates appeared in the late middle Miocene, i.e., during and after the major cooling phase at around 14.5 Ma. This implies that deposition of phosphate and organic carbon continued well after this cooling phase, thereby underlining the observation that preservation of organic carbon in the Monterey Formation is not only dependent on climate change during the mid Miocene but also on regional conditions.

INTRODUCTION

The middle Tertiary is the most recent and best documented time interval in Earth history in which the climate system switched from a ''greenhouse'' into ''icehouse'' mode, with a first step of major cooling in the latest Eocene and Oligocene and a second important cooling phase in the middle Miocene (Vincent and Berger 1985; Miller and Feigenson 1991; Flower and Kennett 1993a, 1993b, 1994a, 1994b; Hodell and Woodruff 1994). A wide variety of mechanisms have been proposed to explain climate cooling, including (1) Himalayan uplift (leading to an increase in erosion, higher CO_2 consumption through increased weathering, higher productivity rates, cooling, etc.; e.g., Raymo et al. 1988; Raymo and Ruddiman 1992; Raymo 1994); (2) isolation of Antarctica (by a circum-Antarctic current system, leading to increased glaciation and cooling; Kennett 1985; Flower and Kennett 1994b), and (3) increased upwelling (leading to more productivity and subsequent cooling = ''Monterey hypothesis''; Vincent and Berger 1985).

The interest of our group is to better understand the middle Miocene cooling step, and especially to test the ''Monterey hypothesis'', which is a pioneering hypothesis involving feedback mechanisms between changes in ocean circulation and climate change (Vincent and Berger 1985). In a first approach, we focus on a selection of key localities of the Monterey Formation, a formation on which the ''Monterey hypothesis'' originally was based. With a mix of detailed stratigraphic, sedimentological, mineralogical, geochemical, and paleontological analyses, we aim at obtaining (1) a better control on the timing and mechanisms of accumulation of phosphate and organic carbon in the Monterey Formation during the late early to early late Miocene age (e.g., Kleinpell 1938, 1980; Blake 1981, 1994; Arends and Blake 1986; Barron 1986a, 1986b; Barron and Keller 1983; Barron and Isaacs 2001; De Paolo and Finger 1991; Flower and Kennett 1993a, 1994a; Echols 1994); and (2) an improved understanding of the general relationships between deposition of organic carbon and phosphate and cooling during the Middle Miocene (John 1999; Badertscher 2000).

One of the key sections in the Monterey Formation is located at El Capitan State Beach (approximately 30 km west of Santa Barbara; Fig. 1). The Monterey Formation is exposed here nearly continuously, from its basal contact with the Rincon Shale to the overlying Sisquoc Formation (e.g., Isaacs 1981; Hornafius 1994a, 1994b; Echols 1994). It is this section, and especially the organic- and phosphate-rich members so well exposed in this outcrop, which we discuss here.

ANALYTICAL METHODS

The section in the Monterey Formation at El Capitan State Beach was logged at centimeter resolution (1997–1998), and sampled at 2-meter intervals for the intervals above and below the phosphate-rich interval, and at 50-cm intervals for the approximately 40 m thick phosphate-rich interval (Figs. 2, 3). Samples were cleaned and cut into two slabs; one half was polished, and the other half was used to make thin sections and powdered samples. The samples to be powdered were ground using a ''jaw'' crusher and an agate mill to obtain powders with a particle size < 40 μm. Between 60 and 100 mg of powdered sample material was used for the characterization of organic matter and the determination of total organic carbon content (TOC) using a Rock-Eval™ 6 (temperature ranges for pyrolysis and oxidation 300–650°C and 400–850°C; heating steps 25°C/min; initial time 3 min; Espitalié et al. 1985). For X-ray diffraction (XRD) bulk-rock

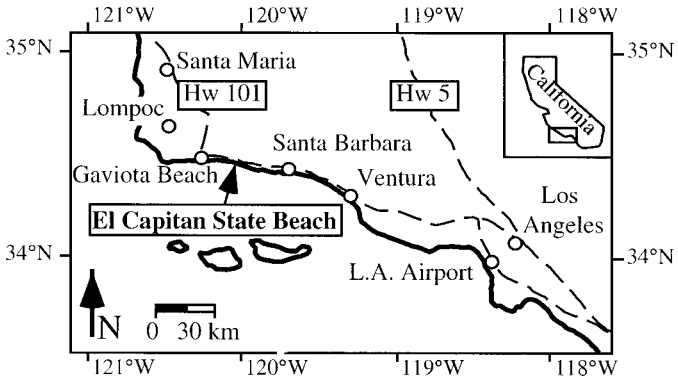

FIG. 1.—Location of the El Capitan State Beach section.

analyses we used a Scintag XRD 2000 diffractometer following the methods described by Ferrero (1965, 1966), Klug and Alexander (1974), and Kübler (1983). XRD clay-mineral analyses were based on methods developed by Kübler (1983, 1987) and Moore and Reynolds (1989). Slides for nannoplankton identification were made using the settling method described in De Kaenel and Villa (1996).

STRATIGRAPHY

The Monterey Formation is usually divided into three members: (1) a lower calcareous member; (2) a middle carbonaceous and phosphate-rich member, and; (3) an upper siliceous member (Bramlette 1946; Isaacs 1981, 1984, 2001; Pisciotto and Garrison 1981; Garrison et al. 1987, Garrison et al. 1990, Garrison et al. 1994; Mackinnon 1989; Hornafius 1991; Behl 1992, 1999; White 1992; White et al. 1992; Chang and Grimm 1999; Chaika and Williams 2001). In the section at El Capitan State Beach, a clear distinction between the lower and middle member using the presence and/or absence of carbonate beds is not possible; also systematic analyses by XRD show no consistent trend in calcite contents which could be used for a distinction. Alternatively, a distinction is possible based on the color and TOC contents of the marls, as will be shown in this paper. The section measured for this study starts where the lower member grades into the middle member and ends approximately 20 m below the base of the upper member (Figs. 2, 3).

We divided the measured section up into five different units, based on the different observed lithologies and mineral distributions (Fig. 2). The ''gray'' marl unit has high quartz content (up to 12.5%) at the base that diminishes rapidly upsection; phosphate content is generally low (max. 25%) and calcite content is variable (max. 78%). The main lithology consists of a grayish marl. In the subsequent ''black'' marl unit, quartz content is generally low (max. 7.3%) and phosphate content is higher (max. 52%); calcite content is variable (max. 62%). The main lithology is a dark-colored marl (''black marl'' in the following). In the ''red'' marl unit, quartz values are high again (max. 12.5%), and also the phosphate values are generally high (max. 90%); calcite content, on the contrary, is usually low and often reach values below detection limits; clay mineral values are generally higher than in the under- and overlying intervals (max. 25%). The main lithology is a reddish marl (or mudstone, where calcite contents are low). The following interval corresponds to the succession of condensed phosphatic beds. The mineral contents are comparable to the ''red'' marl unit, except for the phosphate values, which are usually higher (up to 80%). The uppermost interval described here is similar to the dark marl unit with regard to its mineral composition.

SEDIMENT TYPES AND CONSTITUENTS

The principal minerals identified in the measured section are authigenic, biogenic, and secondary. Authigenic minerals include quartz, ankerite/dolomite, and phosphate (mostly frankolite, minor amounts also of fluorapatite; but compare also Medrano and Piper 1997). The main biogenic mineral is calcite, in the form of calcareous nannofossils and foraminifera. Secondary minerals include halite (probably of modern origin); jarosite ($KFe_3(SO_4)_2.(OH)_6$) found in bentonites (and coloring those orange-brown) and derived from K-rich minerals; gypsum, probably derived from pyrite weathering and/or SO_4-rich fluids reacting with calcite; and K-feldspar and plagioclase which may have originated from volcanic deposition. The amount of nonvolcanic detrital minerals remains in general below detection limits. Discrete occurrences of silt-size quartz grains in the red marl and condensed intervals are related to the presence of agglutinated foraminifera (usually diagenetically compressed).

Marl

Marl is the dominant lithology in the measured section. Three different types of marl have been distinguished (Table 1). The occurrence of ''gray marl'' (grayish color when weathered) is restricted to the lower part of the Monterey Formation and is taken here to define the lower ''calcareous'' member. It's rather high calcite content is due to the abundance of calcareous benthic foraminifera and calcareous nannofossils. The foraminifera are usually concentrated in discrete intervals rather than scattered throughout the sediment. Their shells are often broken (Fig. 4B). Phosphatic layers and lenses are mostly absent, whereas near the overlying ''black'' marl unit, phosphatic coated grains and peloids appear.

At the base of the next unit, the gray marl is replaced by a brown, dark brown, or black marl (''black marl'' in Table 1), which shows higher TOC contents (mean value of 7.5 wt%; Table 1). The organic matter is not uniformly distributed but appears to be enriched in layers and laminae, which are several millimeters to several centimeters thick. Calcareous benthic foraminifera are less abundant than in the gray marl unit. Some foraminifera preserve geopetal structures, which often are not in original position (Fig. 4A). This lithology includes abundant phosphatic particles, light-colored phosphatic layers, lenses, and nodules, which locally occur in concentrated form in discrete intervals.

In the overlying unit, a marl is present that shows a red to brown color when weathered (''red marl''). TOC reaches maximal values (average 15%). Calcareous benthic foraminifera are mostly absent, and agglutinated, quartz-bearing foraminifera are abundant but commonly deformed by compaction (Fig. 4D). The change from calcareous to agglutinated forms is seen in the bulk mineralogy distribution in the marl, with calcite values dropping and quartz values increasing relative to the gray and dark marls (Fig. 2; Table 1). In the case of low calcite values, the red marl becomes a reddish mudstone. Phosphatic layers and nodules are present but usually not as abundant as in the black marl. The observed phosphatic layers are usually more prominent than those in the black marl and are concentrated in discrete intervals, up to 10 cm thick. The phosphate particles are light-colored and may display angular morphologies. Phosphatic lenses and laminae are rare.

Phosphate

The black and red marls include light-colored phosphate layers, lenses and nodules. In addition, multiple-layer, condensed, phosphatic beds appear in the condensed unit (Table 1). On the basis of our field data, polished samples, and thin sections, we are able to distinguish three types of phosphate occurrences:

1. Phosphatic particles of micrometer to millimeter size, which are either coated grains (40–200 μm, with foraminifera, quartz grains, or smaller coated grains as nucleus) or regular and irregular particles without internal structure (''peloids''). The coated grains often show multiple layering, with occasional organic matter interlayering (Fig. 4H). Coated grains may also merge to form larger agglomerates (Fig. 4I). Forami-

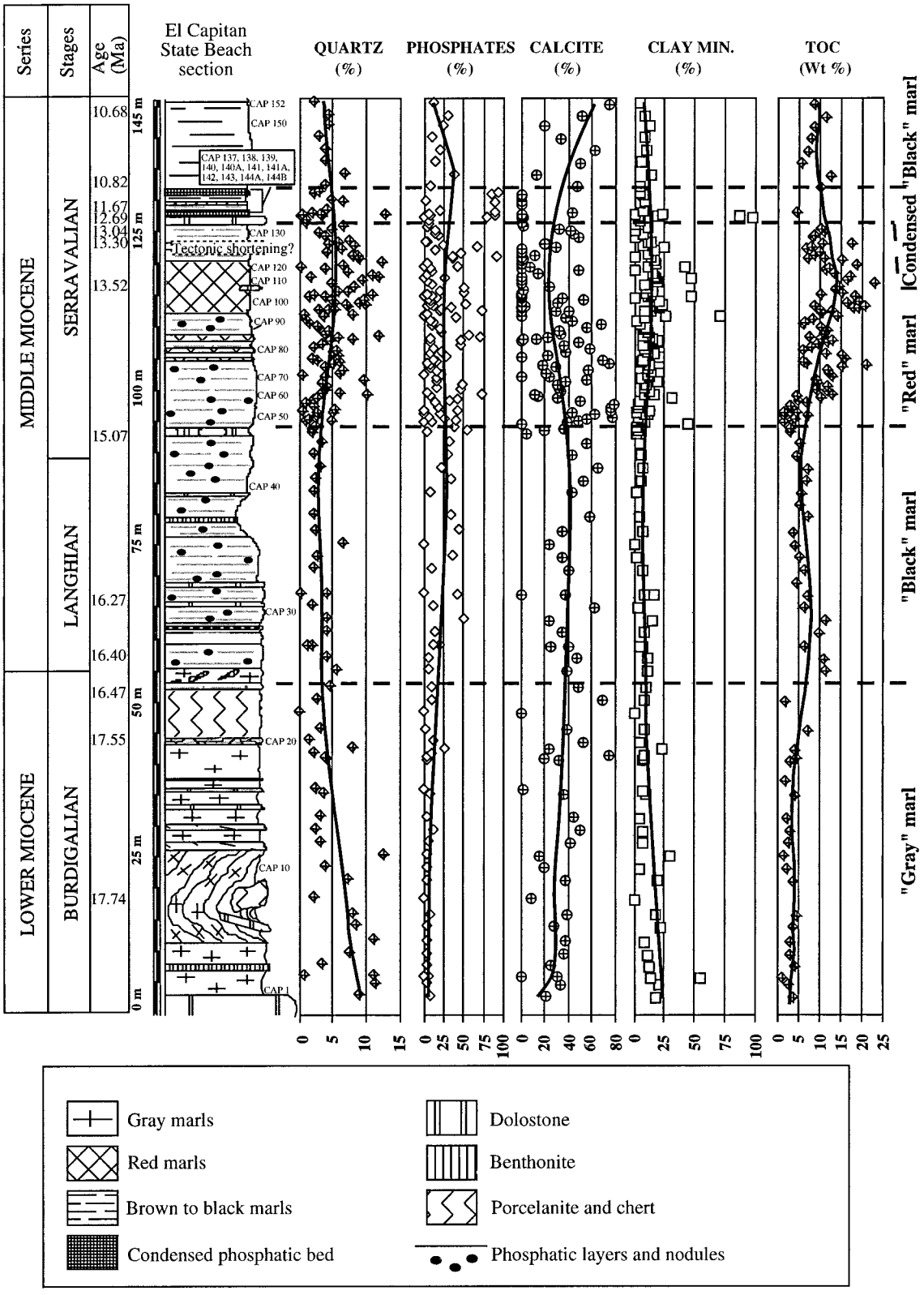

FIG. 2.—Stratigraphic plot of the upper, lower, and middle part of the Monterey Formation at El Capitan State Beach. Positions and ages of calcareous nann ofossil events are from Table 2. The top nannofossil event is obtained by correlation with the nearby section of Naples Beach (Badertscher 2000).

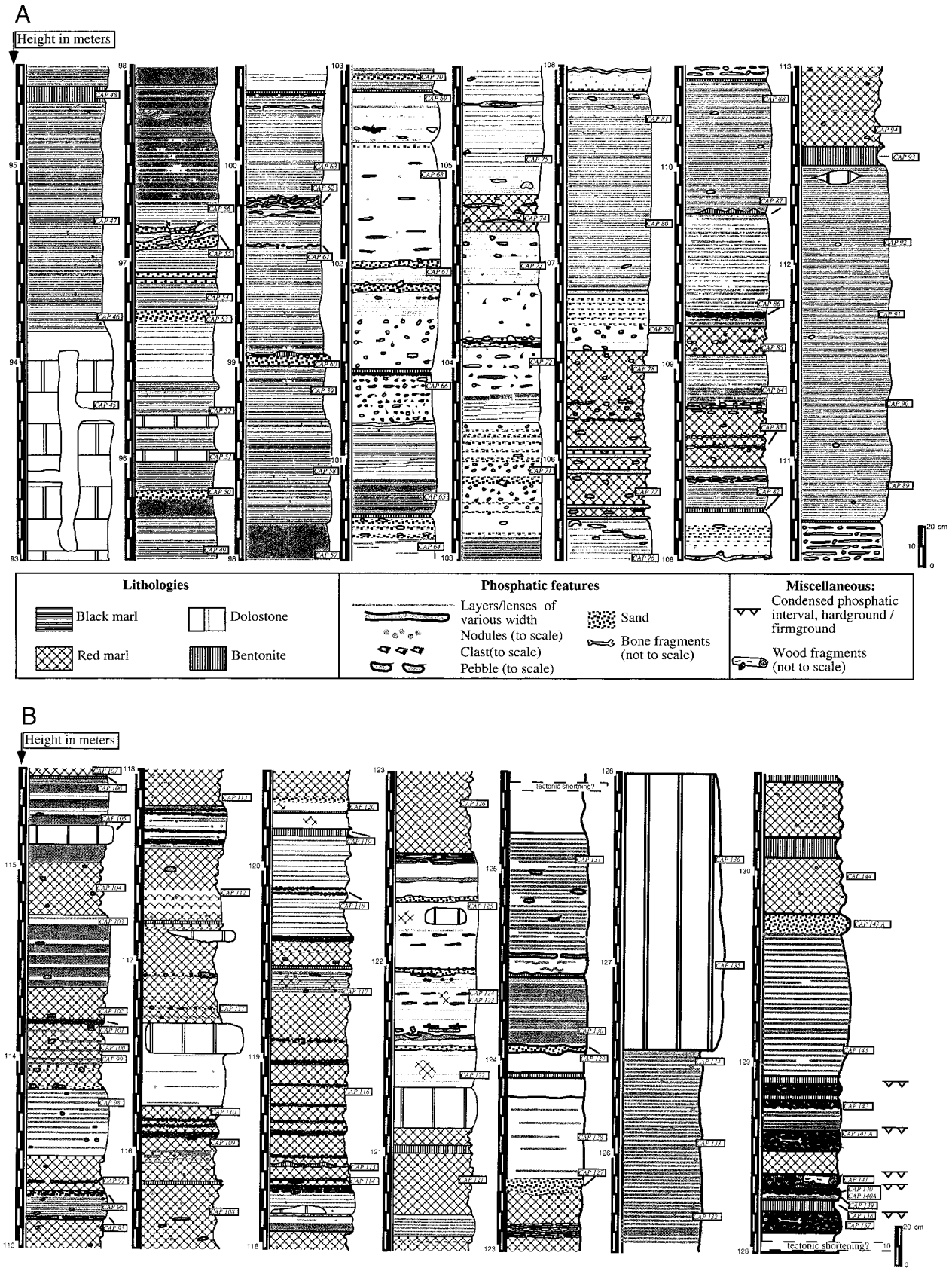

FIG. 3.—Detailed section in the middle, carbonaceous, and phosphate-rich member of the Monterey Formation at El Capitan State Beach showing the distrib ution and sedimentological patterns of phosphates. This section spans the 93 to 130.5 meter interval of the entire measured section (Fig. 2).

TABLE 1.—*Mineralogic characteristics and TOC contents in marl, condensed phosphate, dolomite, and bentonite.*

Lithology	"Gray marl"	"Black marl"	"Red marl"	Condensed phosphate	Dolomite	Bentonite
Occurrence in section	Lower part (0–56 m)	Middle and upper part (56–123 m)	Upper middle part (104–123 m)	Upper middle part (128–132 m)	Throughout the section	Throughout the section
age	> 16.4 Ma	16.4–<10.6 Ma	ca. 14.5–10.8 Ma	ca. 12.7–10.8 Ma		
Number of samples	20	85	27	7	5	10
TOC and mineralogy (range, mean, wt %)						
TOC	1.21–7.46, 2	1.56–17.56, 7.5	7.08–23.23, 15	—	—	—
Quartz	3–12.5, 6.5	0.5–10, 4	2–12, 4	2–13, 4.5	1–2.5, 2	0–2, 1
Phosphate	3–26, 7.5	0–92, 24	5–72, 23	0	0–7.5, 4	0–9, 1
Calcite	15–68, 33.5	0–85, 39	0–39, 5	9–90.5, 77	0–8, 3	0–2, 0.5
Dolomite/ankerite	—	—	—	—	16.5–35.5, 27.5	—
Clay minerals	5–29, 13	0–31, 8.5	8.5–26, 16.5	0–19, 6	0–6.5, 2.5	12–97.5, 52
Gypsum	—	—	—	—	—	0–70.5, 13.5
Observations	Calcareous benthic foraminifera abundant; phosphatic layers and lenses mostly absent	Calcareous benthic foraminifera present; phosphatic layers and lenses present	Calcareous benthic foraminifera mostly absent, agglutinated forms abundant; phosphatic layers and lenses present	Occurs as discrete, sometimes superimposed layers.	Occurs as continuous beds, nodules, and particles.	Occurs as continuous laminae and beds of < 1 mm to max. 40 cm thickness

nifera coated by phosphate are commonly well preserved and do not show signs of compaction as is often the case with their noncoated counterparts (Fig. 4G). Phosphatic particles appear scattered or in concentrations in marl, and may equally be part of light-colored phosphatic lenses and laminae (Figs. 4K), as well as of dark-colored, condensed, phosphatic beds (Figs. 4F, M).

2. Phosphatic nodules, lenses, and laminae, which are composed of light-colored (yellowish to gray), homogeneous, and mostly friable phosphate in which nonphosphatic particles are trapped (such as quartz, foraminiferal tests, etc.; Fig. 4N). In a few cases, the phosphatic matrix may also be more indurated and less friable, thereby retaining its light color. The lenses and laminae may alternatively result from the accumulation and concentration of phosphatic particles. The nodules range from millimeters to several centimeters in size; the lenses, laminae, and layers attain a maximum thickness of 1 cm. The nodules are often well rounded (Fig. 4L), but some may also show well-defined edges. In some cases, the nodules display multiple layers of friable phosphate around a core of indurated phosphate (cf. Fig. 5.5B in Föllmi and Garrison 1991). The phosphatic lenses may show evidence of erosional truncation, most likely by sediment scouring. Phosphatic nodules appear scattered or concentrated in discrete horizons in marl, whereas the phosphatic lenses and laminae are regularly intercalated with marl, or stacked and concentrated in phosphatic horizons.
3. Condensed phosphatic horizons, which are composed of phosphatic nodules, lenses and laminae, and include phosphatic particles. They occur in densely stacked, discrete horizons in interval D, forming phosphatic condensed beds up to 40 cm thick. Their color is mostly beige to dark brown. These beds consist of layers dominated by phosphatic nodules and particles, and layers that are more homogeneous, less nodular, and consisting of a matrix that is thoroughly phosphatized (Fig. 4E). Bone and phosphatized wood fragments are not uncommon in these beds. Phosphatic particles may include geopetals that are partly not in upright position (Fig. 4C). The nodular layers may display inverse grading, with the largest nodules on top (Fig. 4J). The phosphatic horizons often show an increase in concentration and thickness of phosphatic lenses and laminae towards the top (Fig. 4N).

These three types of phosphate occurrence in the Monterey Formation at El Capitan State Beach are end members, with the condensed phosphatic horizons being a product of some sort of combination of the first two types. The first two types of phosphate would correspond to the "pristine phosphate" category of Föllmi et al. (1991; compare also Föllmi and Garrison 1991; Föllmi 1996), with the exception of levels consisting of discrete concentrations of phosphate particles, nodules, and lenses, which would correspond to the "condensed phosphates" category, whereas the last type is identical to the "condensed phosphates" category in Föllmi et al. (1991; with admixtures of probably allochthonous phosphates). The three types discerned here correspond to the three categories "P-phosphates" (peloidal phosphates), "F-phosphates" (friable phosphates), and "D-phosphates" (dark and dense phosphates) of Garrison et al. (1994; compare also Garrison et al. 1987, Garrison et al. 1990; Kolodny and Garrison, 1994).

Other Lithologies

Porcelanite and chert are subordinate lithologies, which commonly occur closely interbedded in the section measured (Isaacs 1981, 1985; Isaacs et al. 1983; Behl 1992). Dolomite is present in continuous beds, nodules (up to 1 m in length), and discrete particles (millimeters to centimeters in size; e.g., Garrison et al. 1984; Burns and Baker 1987). Bentonite occurs in laminae and beds up to 40 cm thick and is common throughout the section (e.g., Hornafius 1994c). Among the clay minerals identified, we found approximately 98% to consist of biotite, smectite, and zeolite (of the clinoptilolite–heulandite series). The remaining 2% include chlorite, kaolinite, and mixed-layer clay.

Organic Matter

TOC contents measured by Rock-Eval show a wide range of values, with values near 0% in certain dolomite and bentonite samples and up to 23% in red marl (Fig. 2). In general, TOC values increase from the gray marl unit to the red marl unit (from 2 to 15 wt % in average; Table 1) and decrease again in the upper black marl unit (to 8 wt %).

Systematic analysis of the hydrogen index versus T_{max} in organic matter of the measured section shows it consistently to be of type II kerogen (Fig. 5). No mixing with type III kerogen has been observed. This may suggest that the source of organic matter is predominantly marine (Summerhayes 1981; compare also Isaacs and Petersen 1987; Stein 1991; Behl 1999). Organic matter preserved in bentonite and dolomite plots in the type III field. The origin of this difference in quality is not clear but may be due to substrate-related differences in postdepositional alteration.

CALCAREOUS NANNOFOSSIL BIOSTRATIGRAPHY

Prior biostratigraphic work on sections in the Monterey Formation is based on benthic foraminifera, diatoms, nannoplankton, carbon, oxygen, and strontium stable isotopes and paleomagnetism (Kleinpell 1938, 1980; Arends and Blake 1986; Blake 1981, 1994; Barron 1986a, 1986b; Barron and Keller 1983; Barron and Isaacs 2001; DePaolo and Finger 1991; Khan-Omarzai et al. 1993; Flower and Kennett 1993a, 1994a; compare also Ingle 1980). Published stratigraphic ages are not always consistent, and, especially for the condensed unit, different age envelopes have been proposed (DePaolo and Finger 1991). We employed calcareous nannofossil

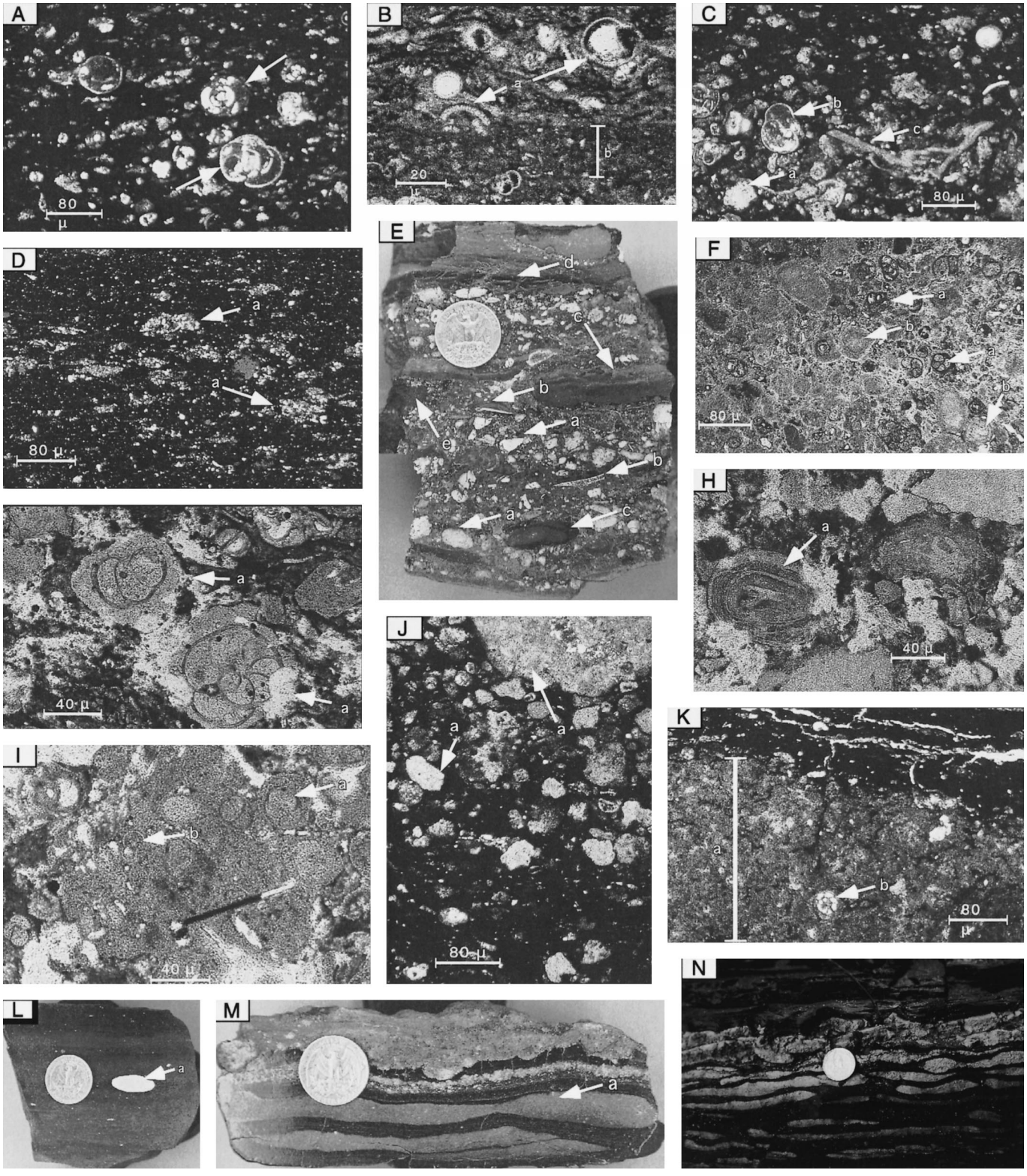

FIG. 4.—**A)** Rotated geopetal structures in foraminifera embedded in dark marl as indicated by white arrows; sample Cap 59. **B)** Accumulation of broken foraminifera (a) in an organic-rich matrix (gray marl); Cap 20. **C)** Condensed microlayer (< 1 mm) composed of phosphatic particles (a), foraminifera (with rotated geopetal structure: b) and bone fragments (c); Cap 59. **D)** Siliceous agglutinated benthic foraminifera (a) preserved in a red marl; Cap 111. **E)** Condensed phosphatic horizon containing light-colored phosphatic nodules (a), bone fragments (b), ''soft'' sediment pebble (organic-rich mudstone = c), organic-rich matrix (d), and wood fragments (e); Cap 144A. **F)** Condensed phosphatic horizon; phosphatic matrix contains phosphatized foraminifera (a) and coated grains (b); Cap 140a. **G)** Foraminifera coated with phosphate (a); Cap 47. **H)** Multilayered phosphate-coated grain (a); Cap 101. **I)** Phosphate-coated grains coalesced into a multi-compound nodule. Individual coated grains (a) and foraminifera (b) are still recognizable; Cap 50. **J)** Concentration of phosphatic particles and nodules (a); Cap 128. **K)** a cohesive phosphatic level overlain by an organic-rich layer; b = benthic foraminifer; Cap 62. **L)** Large phosphatic nodule (a) in a dark and homogeneous marl; Cap 130. **M)** Superimposed phosphatic layers (a) in an organic-rich matrix; Cap 62. **N)** Phosphatic lenses increasingly densely packed toward the top, probably because of winnowing events of increasing strength; Cap. 62.

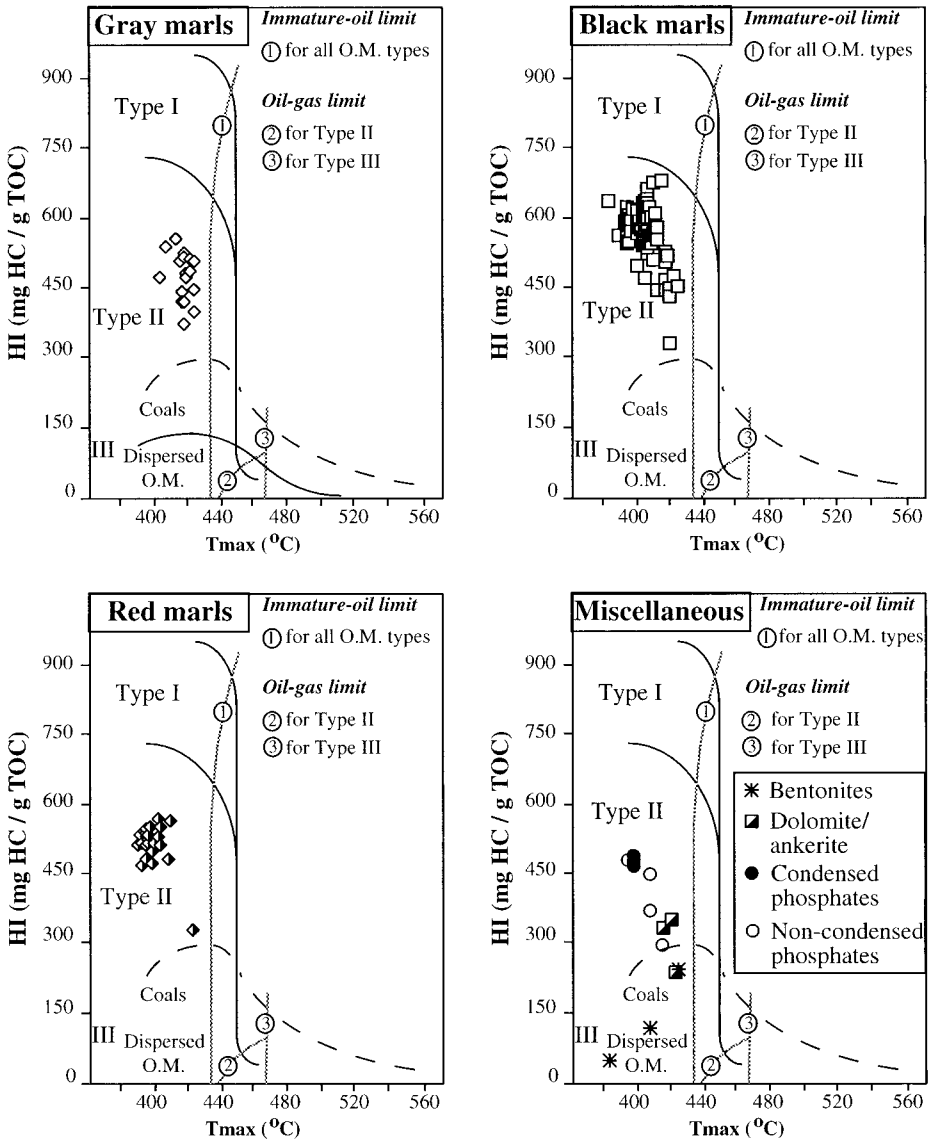

FIG. 5.—Hydrogen index versus Tmax for organic matter in gray, black, and red marls, as well as in miscellaneous constituents of the Monterey Formation at El Capitan State Beach, measured with a Rock-Eval™ 6.

biostratigraphy in order to obtain a biostratigraphic time frame with sufficient resolution. The application of nannofossil biostratigraphy combined with orbitally tuned time scales for the younger part of the Miocene has resulted in improvements in age calibration. Miocene bio-events may have uncertainties as low as ± 2 ky (in average ± 7 ky, see e.g., Backman and Raffi 1997; Hilgen et al. 2000).

Abundance and Preservation

Marl samples with sufficiently high levels of calcite (> 20%; selected by X-ray analyses) provided identifiable nannofossil assemblages, which offered sufficient bio-events in order to construct a zonal scheme for the El Capitan State Beach section (Tables 2, 3, Figs. 6–9). The preservation of calcareous nannofossils (Fig. 6) varies from poor (severe dissolution, fragmentation, and/or overgrowth of specimens) to mixed (dissolution/and or overgrowth is present, but up to 95% of specimens can be identified with certainty). In the lower part of the section, between 0 and 112 meters, preservation is generally moderate to mixed. In the upper part of the section, between 112 and 146 meters, preservation is poor to moderate. The following code has been used for estimations of the relative abundance of individual taxa:

P (present): 1 to 2 specimens per 201–500 fields of view.

R (rare): 3 to 14 specimens. One specimen per 51–200 fields of view.

F (few): 15 to 74 specimens. One specimen per 11–50 fields of view.

C (common): 75 to 150 specimens. One specimen per 2–10 fields of view.

A (abundant): 151 to 1000 specimens. 1–10 specimen per field of view.

O (ooze): 1001 to 5000 specimens. > 10 specimens per field of view.

The total abundance of calcareous nannofossils in the measured section varies from few to ooze (Fig. 6).

Zonal Scheme

The standard biostratigraphic scheme of Martini (1971) has some limitations in the Monterey basin because of the rarity of zonal markers such as *Helicosphaera ampliaperta, Sphenolithus heteromorphus, Discoaster kugleri,* and *Catinaster coalitus.* However, markers employed in the zonation of Okada and Bukry (1980) were observed and used to zone the El Capitan State Beach section. These bioevents are the acme in *Discoaster deflandrei, Calcidiscus macintyrei,* and *Cyclicargolithus floridanus.* Alternative biohorizons were also used to define the biozones of Martini (1971) such as the *Sphenolithus heteromorphus* paracme, the *Helicosphaera walbersdor-*

TABLE 2.—*Summary of stratigraphic sections considered for the estimation of ages of calcareous nannofossil events.*

Standard Biohorizons/Secondary Events	Estimated Age in Ma		Reference Sections
FO *Discoaster pentaradiatus*	9.297	1	ODP Leg 94, Site 608
FO *Discoaster brouweri*	10.687	2	ODP Leg 154, Site 926
LO *Discoaster micros* transition	10.790	2	ODP Leg 154, Site 926
LO *Coccolithus miopelagicus* (= FO *Catinaster coalitus*)	10.794	2	ODP Leg 154, Site 926
FO *Discoaster micros* transition	10.820	2	ODP Leg 154, Site 926
LO *Discoaster kugleri*	11.520	2	ODP Leg 154, Site 926
FO-LO *Discoaster kugleri* (middle point)	11.675	2	ODP Leg 154, Site 926
FO *Discoaster kugleri*	11.831	2	ODP Leg 154, Site 926
LCO *Cyclicargolithus floridanus*	12.697	3	ODP Leg 149, Site 900
FO *Triquetrorhabdulus rugosus*	13.043	1	ODP Leg 94, Site 608
LO Discoaster petaliformis	13.307	3	ODP Leg 149, Site 900
Dominance shift *Cyclicargolithus floridanus-Reticulofenestra pseudoumbilicus* (>8.0) (= LO *Sphenolithus heteromorphus*)	13.523	2	ODP Leg 154, Site 926
FO *Discoaster petaliformis*	15.068	3	ODP Leg 149, Site 900
LCO *Discoaster deflandrei*	16.273	3	ODP Leg 149, Site 898
Base paracme *Sphenolithus heteromorphus*	16.40	3	ODP Leg 149, Site 900
LCO *Helicosphaera ampliaperta*	16.479	3	ODP Leg 149, Site 900
FO *Calcidiscus premacintyrei*	17.555	3	ODP Leg 149, Site 900
FO *Discoaster variabilis*	17.744	3	ODP Leg 149, Site 900

1. Age estimation based on Gartner 1992.
2. Backman and Raffi 1997.
3. Age estimation based on De Kaenel and Villa 1996.

TABLE 3.—*Age of biostratigraphic datums in the Monterey Formation at El Capitan State Beach.*

Standard Biohorizons/Secondary Events	Estimated Age in Ma	Depth (m)	Sedimentation rate (m/My)	
FO *Discoaster pentaradiatus*	9.297	160.00	11.20	58.17
FO *Discoaster brouweri*	10.687	144.42	105.14	
LO *Coccolithus miopelagicus*	10.794	133.17	4.64	2.92
FO-LO *Discoaster kugleri* (middle point)	11.675	129.08	2.53	
LCO *Cyclicargolithus floridanus*	12.697	126.49	2.51	
FO *Triquetrorhabdulus rugosus*	13.043	125.62	2.00	
LO *Discoaster petaliformis*	13.307	125.09	45.79	45.79
Dominance shift *Cyclicargolithus floridanus-Reticulofenestra pseudoumbilicus* (>8.0) (= LO *Sphenolithus heteromorphus*)	13.523	115.20	14.92	18.42
FO *Discoaster petaliformis*	15.068	92.15	21.93	76.15
LCO *Discoaster deflandrei*	16.273	65.72	64.72	
Base paracme *Sphenolithus heteromorphus*	16.40	57.50	85.82	
LCO *Helicosphaera ampliaperta*	16.479	50.72	6.06	
FO *Calcidiscus premacintyrei*	17.555	44.02	147.46	
FO *Discoaster variabilis*	17.744	16.15		

Sedimentation rates are calculated between each datum and average rates are indicated for five intervals.

fensis FO (first occurrence), the *Reticulofenestra pseudoumbilicus* (> 8 μm) FCO (first common occurrence), the *Cyclicargolithus floridanus* LCO (last common occurrence), the *Calcidiscus premacintyrei* LCO, the *Calcidiscus macintyrei* (> 11 μm) FO, the *Coccolithus miopelagicus* LO (last occurrence), and the *Discoaster brouweri* FO (Fig. 7).

The here presented calcareous nannofossil stratigraphy of the section is based on the results of thirty-five samples (see Appendix 1). The strati-

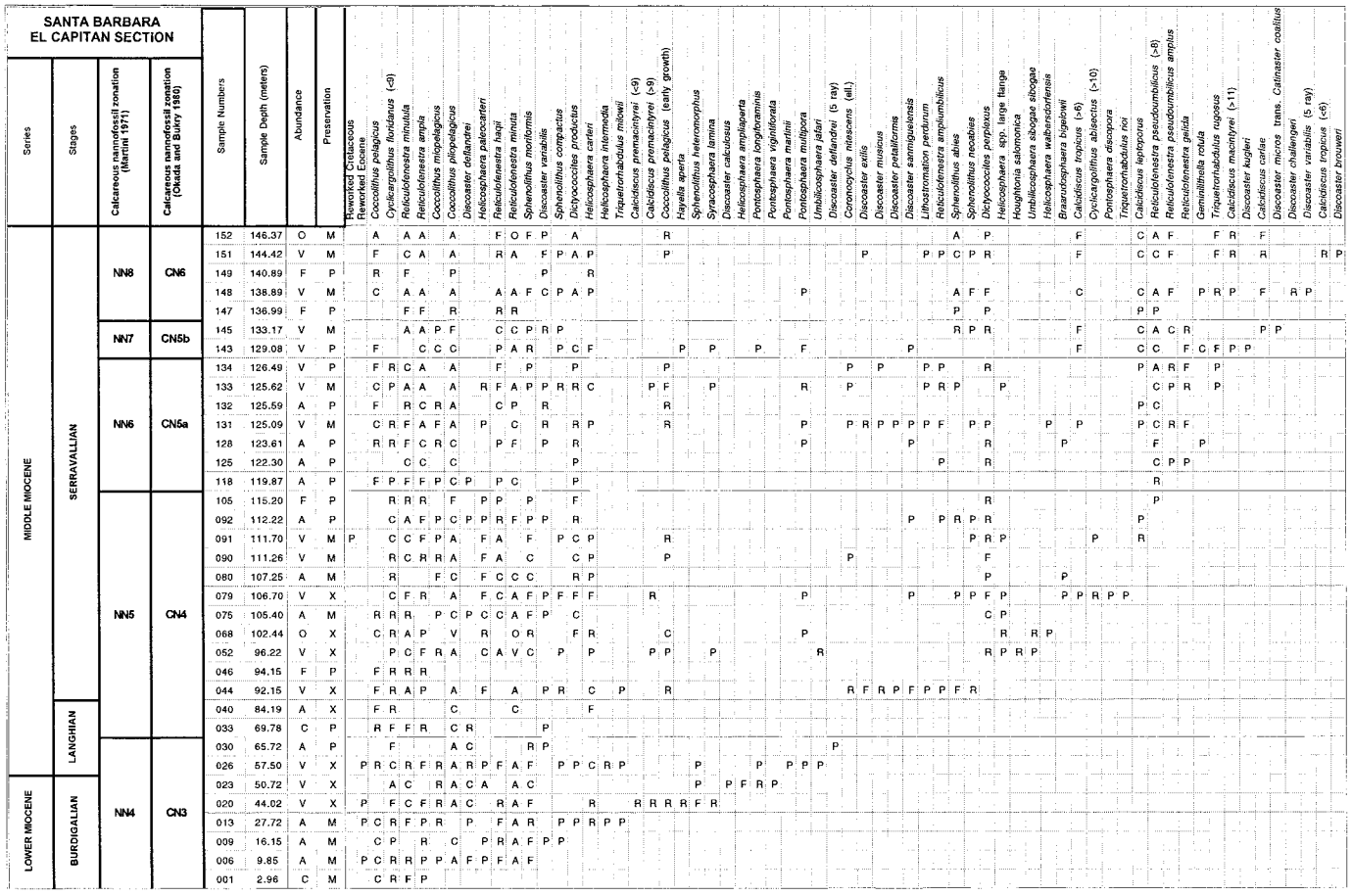

FIG. 6.—Neogene calcareous nannofossil distributions and zonations used to date the Monterey Formation at El Capitan State Beach. Both standard nannof ossil zonations of Martini (1971) and Okada and Bukry (1980) are indicated for reference.

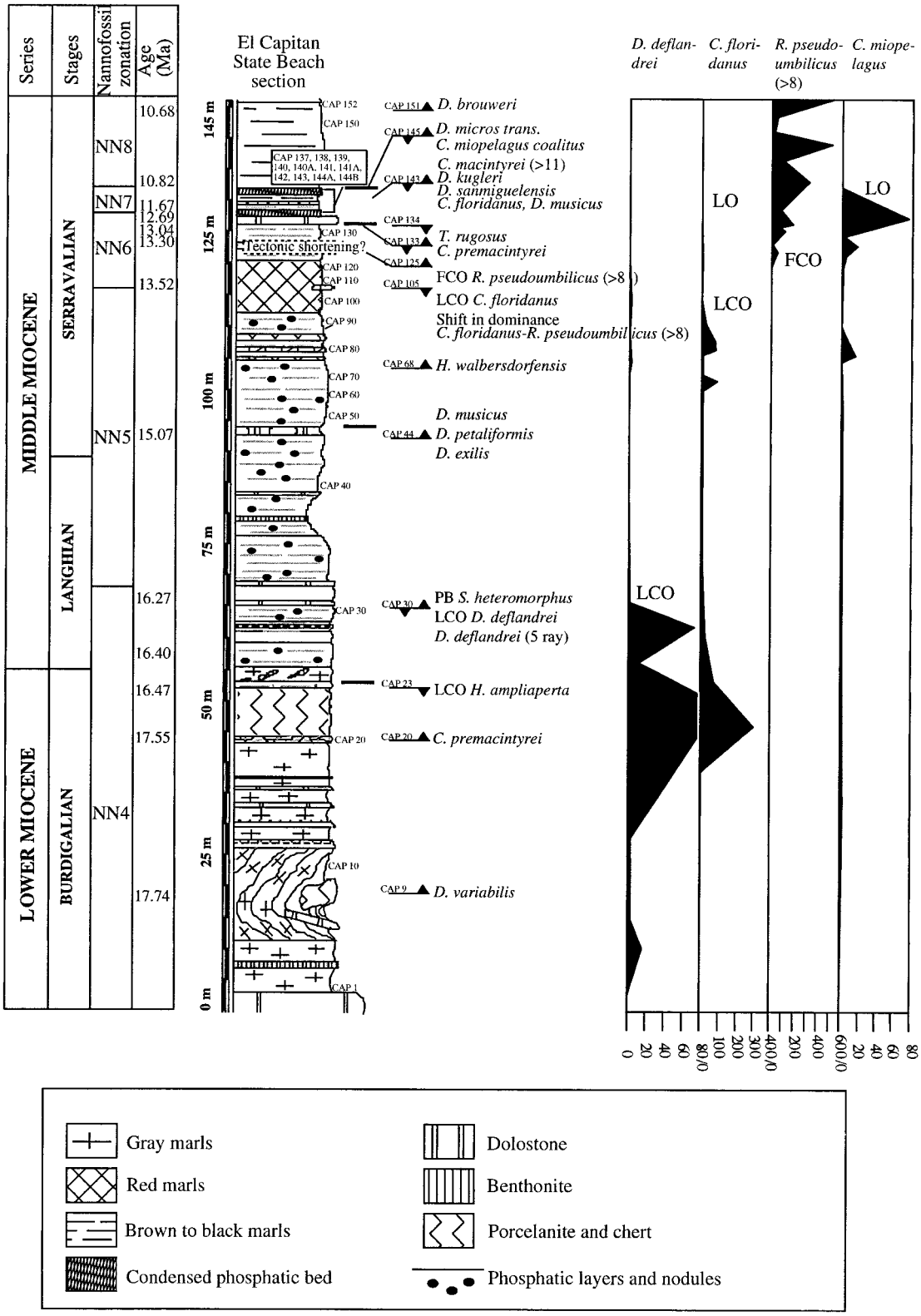

FIG. 7.—El Capitan State Beach lithology and nannofossil bioevents used to zone the section. Semiquantitative counts of species used to zone the section based on abundance variations are indicated. Note that the first occurrence of *Discoaster variabilis* is within a slumped interval.

graphic interval covered by the samples is early to middle Miocene. Based on the zonal scheme of Martini (1971) this interval ranges from the lower part of Zone NN4 to the upper part of Zone NN8. One datum obtained at the nearby Naples Beach section (Badertscher 2000) has been included in order to better constrain the sediment accumulation rate curve (Table 3; Fig. 9).

INTERPRETATIONS

Sedimentation Curve

Using the nannofossil datums as reference points (Appendix 1), the age–depth relationships for the measured section at El Capitan State Beach were plotted (Fig. 9). From 16.48 Ma to 16.27 Ma, the sedimentation rate varied between 85 m/My and 65 m/My. It dropped at approximately 20 m/My. around 15.07 Ma. This rate persisted until 13.31 Ma. From 13.31 Ma onward, it drastically decreased to a rate of 1.96 m/My. The rate calculated for the interval with the condensed phosphatic horizons (12.70 Ma to 10.805 Ma) corresponds to around 3 m/My. Therefore, although real hardground formation was starting at around 12.70 Ma, condensation started already in the red marl unit and is not restricted to the condensed phosphatic unit alone. The sediments immediately above the condensed unit have an estimated rate of around 9m/My.

Phosphogenesis and Phosphate Accumulation

The three end-member types of phosphates identified in the El Capitan State Beach section and described above are genetically related. Whereas the phosphate particles are an expression of local phosphogenesis, mostly around a nucleus, the phosphate laminae and lenses result from laterally extended phosphogenesis, which led to the formation of stratiform zones of phosphate deposition. The phosphate laminae and lenses may include phosphatized particles. The phosphatic condensed horizons include both phosphatic particles as well as lenses and laminae, which form densely stacked, discrete layers, commonly with rather complex internal stratification architectures (Fig. 4E; Garrison et al. 1987; Garrison et al. 1990; Garrison et al. 1994; Föllmi and Garrison 1991; Föllmi et al. 1991).

Several sedimentological features point to the importance of erosion and reworking:

1. Phosphate particles may occur greatly enriched in discrete horizons, a few millimeters to centimeters thick. This phenomenon is explained here by selective erosion of marl (winnowing). In some cases layers composed of phosphate particles show inverse grading, which may be related to the effect of kinetic sieving in gravity-induced grain-flow type transport and deposition, or to the exposure of the bed to progressively stronger winnowing events (Föllmi et al. 1991). Layers concentrated in phosphate particles may include foraminifera with tilted geopetal structures (Fig. 4C), interpreted as the result of sediment reworking.
2. The contact of the phosphate layers and lenses with the overlying sediments may be marked by shallow incisions, which may even lead to an interruption of a phosphate layer. These incisions are interpreted here as shallow scours, resulting from erosion.
3. Well rounded, white colored, and mostly friable phosphate nodules (millimeters to several centimeters in size) occur isolated in marl. In some layers such nodules may include distinct cores of more indurated phosphate (Föllmi and Garrison 1991). These nodules are interpreted here to be allochthonous and transported within marly mud flows.
4. The condensed phosphate beds show different indications of sediment reworking, including fracturing and reworking of phosphate laminae, heterogeneous mixtures of phosphate particles, the presence of different phosphate generations around nodules, and the presence of erosional structures. Sometimes condensed horizons tend to consist of progressively concentrated phosphate lenses and laminae, pointing to an intensification of concentration processes during their formation.

These observations suggest that phosphogenesis took place mainly close to the sediment–water interface, and that sediment reworking events and episodes were instrumental in the concentration and stratification of the phosphate-rich horizons. In a model proposed here for the formation of the condensed phosphate beds, we assume an interplay of sediment deposition, phosphogenesis, and sediment erosion, along the following lines (Fig. 10):

1. Initially, a marl is present, which is composed mainly of fine-grained organic matter, clay minerals, nannofossil ooze, and siliceous organisms, and which contains benthic foraminifera.
2. The benthic foraminifera and other particles near the top of the marly bed become concentrated through a winnowing event and undergo coating and phosphogenesis (microbially mediated? e.g., Reimers et al. 1990).
3. The thus coated and phosphatized particles may become further enriched by repeated winnowing events and form layers of up to several centimeters thickness. Inverse grading may result from kinetic sieving during gravity-flow deposition or by progressively stronger winnowing events.
4. Due to a prolonged stay of these concentrated layers at or near the sediment–water interface, phosphogenesis may continue and cement the layers concentrated in phosphate-coated grains.
5. High-energy events (strong currents but also seismic events; Seilacher 1969; Grimm and Orange 1997) may lead to the rupture of such layers and the formation of phosphate intraclasts, which may be incorporated into the condensed layers.

Some sort of combination of these phases, as well as their repetition, may have led to the formation of most of the condensed phosphate layers observed in the Monterey Formation at El Capitan State Beach.

Accumulation of Organic Matter

The degree of preservation of organic matter and the type of lithology present in the Monterey Formation at El Capitan State Beach are interrelated. Whereas the gray marl contains only moderate amounts of organic matter (average 2 wt % TOC), average TOC contents in the black (7.5 wt %) and red marl (15 wt %) are significantly higher. In terms of the stratigraphic distribution of organic matter accumulation, the following is observed:

1. Until around 16.3 Ma, the deposition of gray marl characterized by moderate TOC contents prevailed. Phosphogenesis and the formation of phosphate-enriched intervals was of only subordinate importance. Overall sedimentation rates were rather high (around 75 m/My). By assuming an average marl density of 1.3 g/cm^3 (Badertscher 2000) and using the average TOC content in gray marl, we obtain an average TOC accumulation rate of 0.19 mg/cm^2/yr (cf. Isaacs 2001).
2. From 16.3 until around 14.5 Ma, deposition of black marl dominated. TOC contents increased per sediment unit and phosphogenesis and phosphate accumulation became dominant processes. Overall sedimentation rates decreased to an average level of around 20 m/My, and the average TOC accumulation rate remained at 0.19 mg/cm^2/yr.
3. From around 14.5 to 12.7 Ma, deposition of red marl prevailed and TOC preservation rates per sediment unit reached maximum values. Overall sedimentation rates remained around 20 m/My until around 13.3 Ma (TOC accumulation rate $=$ 0.39 mg/cm^2/yr) and then dramatically decreased to the low rate of around 2m/My (TOC accumulation rate $=$ 0.04 mg/cm^2/yr).
4. From 12.7 Ma to 10.8 Ma, condensation processes prevailed, leading to the formation of a row of phosphatic condensed intervals. TOC preservation rate was very low within the hardgrounds. Overall sedimentation rates were around 3 m/My.
5. From 10.8 Ma onward, sedimentation rates returned to normal values and processes of phosphogenesis gradually became less important. The type of lithology deposited on top of the condensed intervals is a black

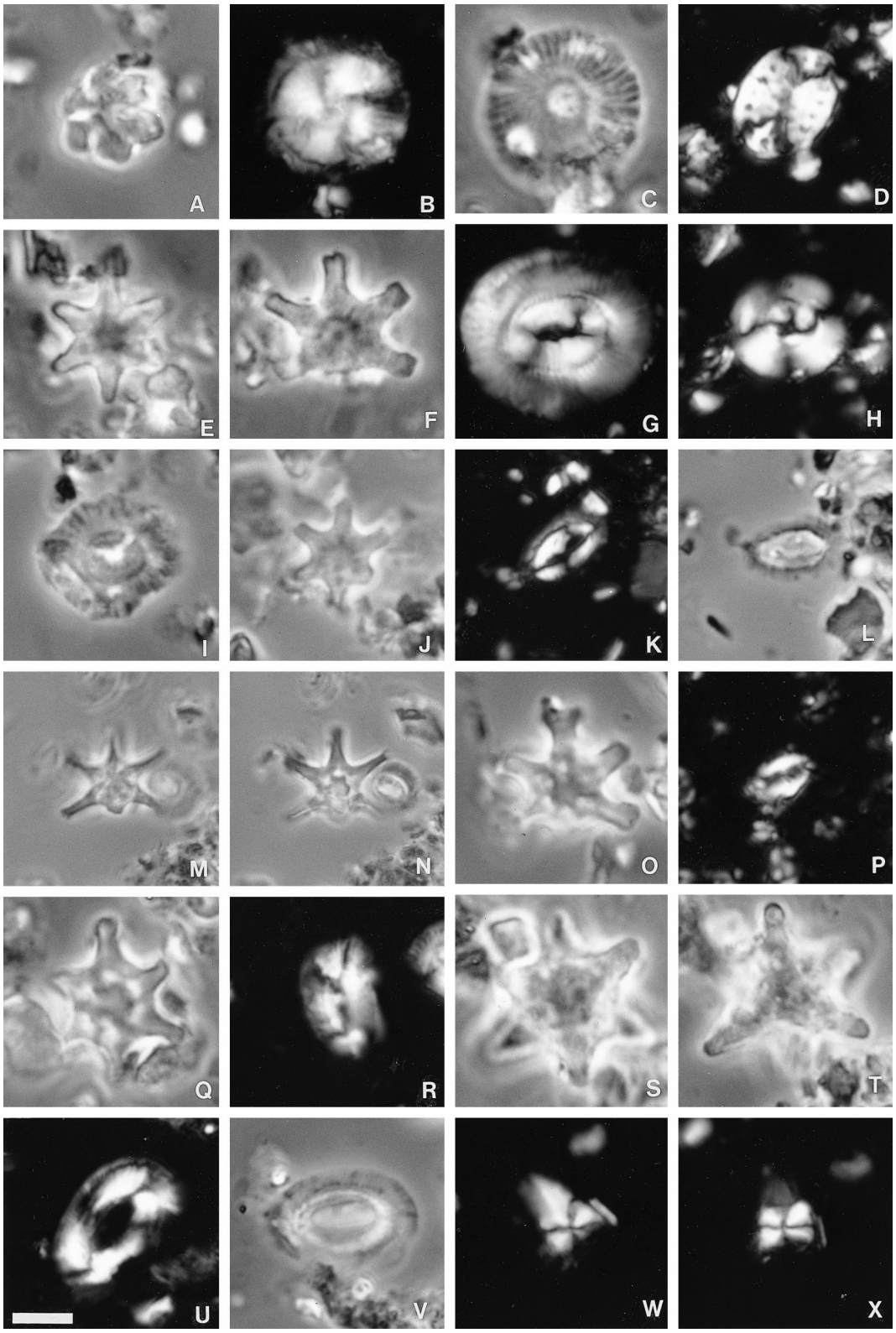

FIG. 8.—Light microscope micrographs of calcareous nannofossils. XP = cross polarized light; Ph = phase contrast. 1 cm = 40 μm in all photos, see scale bar in lower left corner of photo U. Nannofossils are organized according to stratigraphic occurrences from the top left of the section (A) to the bottom right (X). **A)** *Discoaster micros* Theodoridis transitional *Catinaster coalitus* Martini and Bramlette (*sensu* Backman and Raffi). Sample Cap 145, 133.17 m, Ph. **B, C)** *Calcidiscus macintyrei* (Bukry and Bramlette) Loeblich and Tappan, (> 11 μm, circular). Cap 143, 129.08 m, XP (B) and Ph (C), placolith length 11.05 μm. **D)** *Pontosphaera longiforaminis* (Baldi-Beke) De Kaenel and Villa. Cap 143, 129.08 m, XP. **E)** *Discoaster* cf. *D. sanmiguelensis* Bukry. Cap 143, 129.08 m, Ph. **F)** *Discoaster kugleri* Martini and Bramlette. Cap 143, 129.08 m, Ph, specimen with central knob. **G)** *Coccolithus miopelagicus* Bukry. Cap 143, 129.08m, XP (placolith length 13.2 μm). **H)** *Cyclicargolithus floridanus* (Roth and Hay in Hay et al.) Bukry. Cap 133, 125.62 m, XP. **I)** *Calcidiscus premacintyrei* Theodoridis. Cap 133, 125.62 m, Ph. **J)** *Discoaster sanmiguelensis* Bukry. Cap

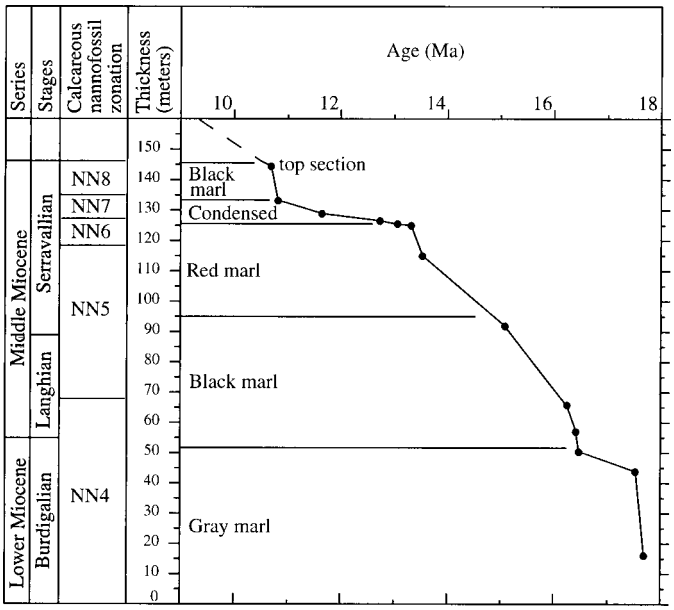

FIG. 9.—Age depth plot of the measured section in the Monterey Formation at El Capitan State Beach, based on 14 identified calcareous nannofossil events (Tables 2, 3). The top nannofossil event is based on the nearby section at Naples Beach (Badertscher 2000) and is used to better calculate the accumulation rate of the uppermost middle Miocene part of the section. Note also that sedimentation rate for the lowermost interval is a maximum value based on the first occurrence of *Discoaster variabilis* in a slumped interval (Fig. 9).

marl. The TOC accumulation rate took up again to an estimated 0.09 mg/cm^2/yr.

A preservation model of organic matter in the Monterey Formation at this site should take the following elements into consideration:

1. On the basis of Rock-Eval analysis the type of organic matter appears to be mainly of marine character, without major terrestrial admixtures (e.g., Stein 1991).
2. High TOC values in the black and red marl units do not necessarily correspond to high TOC accumulation rates, because of the overall low sedimentation rates.
3. Black and red marls were deposited in a dynamic sedimentary environment, in which sedimentation was rather discontinuous (as shown by the presence of phosphate-rich horizons, erosional scours, and allochthonous components).
4. Gray and black marls contain benthic calcareous foraminifera, whereas the red marl mostly lacks benthic calcareous foraminifera and contains abundant agglutinated benthic foraminifera, which may be related to more severe dysaerobic conditions.

Without being able to present a thorough model of organic-matter preservation, we suggest the following conditions to be instrumental to the delivery and conservation of organic matter.

1. Primary productivity rates were probably high, as is indicated by the partly abundant presence of siliceous organisms (e.g., White 1992; White et al. 1992).
2. High productivity rates led to the presence of an oxygen minimum zone, which created dysaerobic conditions at the sea floor, especially during deposition of the red marl.
3. Dynamic conditions during sedimentation of the organic-rich sediments may have led to important sediment reworking and loss of a major part of the organic-rich sediments, as is indicated by sedimentary structures and the low sedimentation rates.
4. Organic-matter preservation was probably enhanced by the early diagenetic formation of phosphate-rich layers and laminae, thereby acting as a semipermeable diagenetic lid, as well as by rapid whole-layer depositional processes (in the form of mud flows) into more dysaerobic environments.

The Monterey Formation and the Monterey Hypothesis

The Miocene is a key interval in our understanding of Cenozoic climate development. The middle Miocene is marked by a major cooling step, which is recorded by a negative excursion in the benthic oxygen isotope record. This negative shift in oxygen isotopes is preceded by a positive shift in δ^{13}C (Vincent and Berger 1985; Flower and Kennett 1993a, 1993b; 1994a, 1994b; Hodell and Woodruff 1994). The pronounced cooling phase has been explained by the so-called ''Monterey event'', where the positive shift in carbon isotopic values is regarded as the product of a direct link between polar cooling, intensified upwelling, high productivity, atmospheric CO_2 drawdown through increased organic-matter burial on the sea floor, and further cooling in a positive feedback loop (Vincent and Berger 1985). According to Vincent and Berger (1985), this loop stopped when oceanic nutrient reservoirs were depleted.

At the center of this model is the lower to upper Miocene Monterey Formation of the central Californian borderland and related formations that were deposited around the Pacific rim. With regard to the Monterey Formation, peak accumulation of organic carbon was hitherto thought to have occurred before the phase of major cooling, i.e., before around 14.5 to 14.1 Ma (Isaacs and Petersen 1987; Pisciotto and Garrison 1981; compare also Raymo 1994), in phase with the positive shift in δ^{13}C (Vincent and Berger 1985). Our new age dates suggest that the sediment intervals with the highest TOC contents and a maximum in TOC accumulation rates appeared in the late middle Miocene, between 14.5 and 13.3 Ma, i.e., during and after the major cooling phase. It should be noted, however, that these intervals are characterized by important condensation, and that overall TOC accumulation rates remained relatively low, when compared to sediments associated with the present-day site of upwelling and high productivity along the Peru margin (9–12 mg/cm^2/yr; Reimers and Suess 1983; compare also Isaacs 2001; Filippelli and Delaney 1992, 1994; Filippelli et al. 1994).

It also remains to be seen to what extent our findings can be extrapolated to other depositional sites of the Monterey Formation. Many authors have already pointed out that facies zones in the Monterey Formation are time-transgressive (e.g., Pisciotto and Garrison 1981; Isaacs 2001), which renders correlation difficult without good time control. Preliminary correlations with the nearby Naples Beach section already show a difference in time for the onset of the unit with highly condensed phosphatic beds (12.7 Ma versus 13.3 Ma; Badertscher 2000). At any rate, deposition of phosphate and organic carbon continued well after the cooling phase at this site, which—if extrapolated to a wider scale—would signify that the data presented here are less supportive of a scenario in which the Monterey For-

←

131, 125.09 m, Ph. **K, L)** *Helicosphaera walbersdorfensis* Müller. Cap 131, 125.09 m, XP, 45° (K) and Ph (L). **M, N)** *Discoaster* cf. *D. bollii* (*sensu* Theodoridis). Cap 131, 125.09 m, Ph, low focus (M) and Ph, high focus (N). **O)** *Discoaster variabilis* Martini and Bramlette. Cap 131, 125.09 m, Ph. **P)** *Helicosphaera* cf. *H. walbersdorfensis* Müller. Cap 68, 102.44 m, XP, 45°. **Q)** *Discoaster musicus* Stradner. Cap 44, 92.15 m, Ph. **R)** *Helicosphaera carteri* (Wallich) Kamptner. Cap 26, 57.50 m, XP, 0°. **S, T)** *Discoaster* spp. (6 rays). Cap 26, 57.50 m, Ph, low focus (S) and Ph, high focus (T). **U, V)** *Helicosphaera ampliaperta* Bramlette and Wilcoxon. Cap 23, 50.72 m, XP, 45° (U) and Ph (V). **W, X)** *Sphenolithus heteromorphus* Deflandre. Cap 20, 44.02 m, XP, 45° (W) and XP, 0° (X).

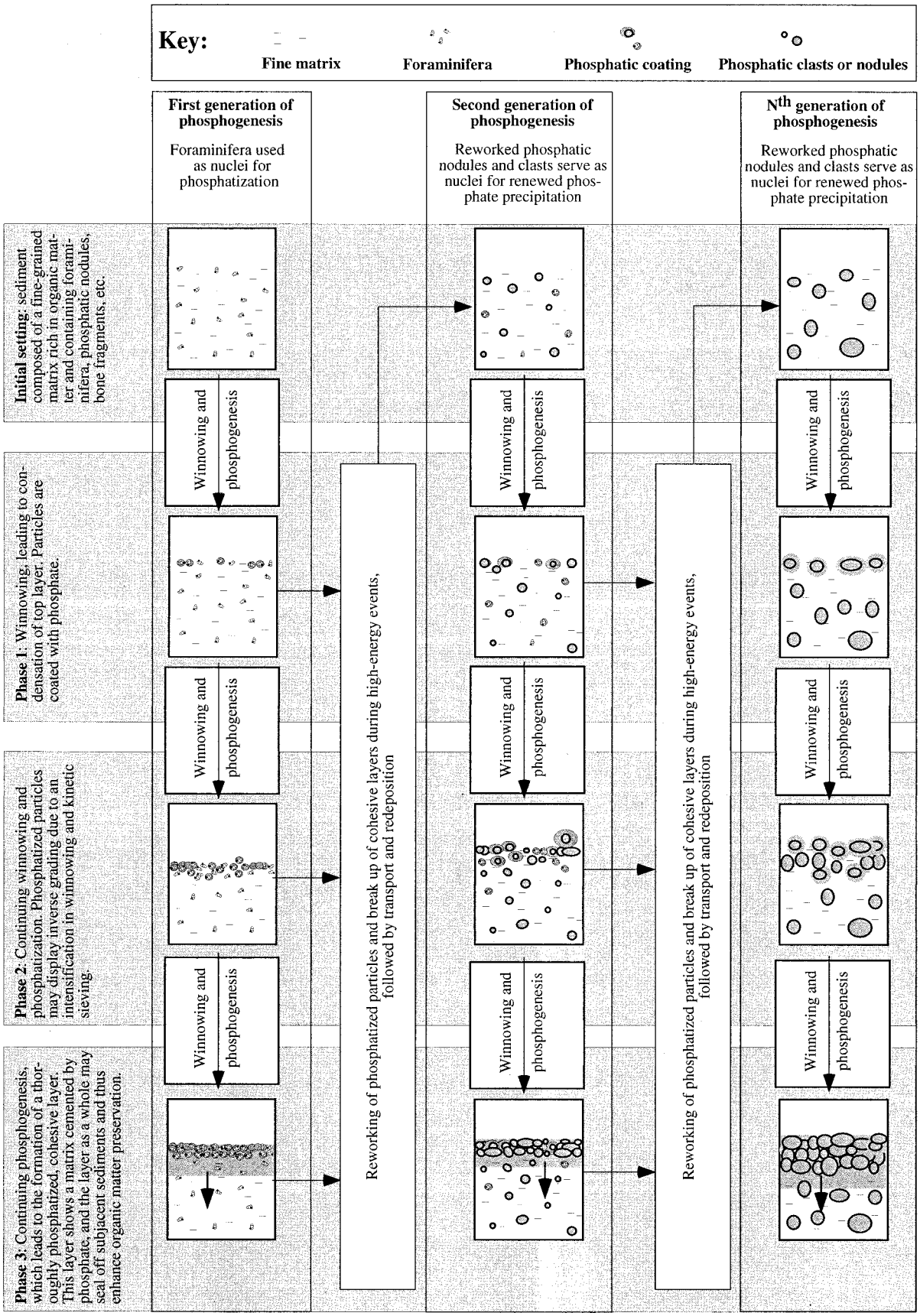

FIG. 10.—Proposed model for the formation of phosphates and phosphatic condensed beds in the Monterey formation at El Capitan State Beach. See text for ex planation.

mation is seen as an important sink for atmospheric CO_2 during the early middle Miocene (cf. also Pagani et al. 1999), which became less efficient after the middle Miocene cooling phase. On the contrary, our data suggest that rates of preservation of organic carbon remained comparable and even slightly increased during and after the cooling phase.

ACKNOWLEDGMENTS

We would like to thank Gerard Magranville for thin-section preparation and Jose Richard for clay minerals preparation. We also thank Rick Behl for guiding us in the field, and Caroline Isaacs, Robert Garrison, Rick Behl, John Barron, and Kurt Grimm for their advice and invaluable insights. We are grateful for the thorough reviews by Marc Hendrix and Kurt Grimm, as well as the editorial remarks by Rick Murray, David Budd, and John Southard, which very much helped to improve the manuscript. Funding for this study was provided by the ''Fond Marguerite Wüthrich et Mattey-Dupraz'' of the University of Neuchâtel.

REFERENCES

Arends, R.G., and Blake, G.H., 1986, Biostratigraphy and paleoecology of the Naples Bluff coastal section based on diatoms and benthic foraminifera, *in* Casey, R.E., and Barron, J.A., eds., Siliceous Microfossils and Microplankton of the Monterey Formation and Modern Analogs: SEPM, Pacific Section, Special Publication 45, p. 121–135.

Backman, J., and Raffi, I., 1997, Calibration of Miocene nannofossil events to orbitally tuned cyclostratigraphies from Ceara Rise, *in* Shackleton, N.J., Curry, W.B., Richter, C., and Bralower, T.J., eds., Proceedings of the Ocean Drilling Program, Scientific Results: v. 154, p. 83–99.

Badertscher, C., 2000, La Formation de Monterey (Miocène) à ''Naples Beach'', Santa Barbara, Californie: une approche sédimentologique, mineralogique et géochimique [unpublished diploma thesis]: University of Neuchâtel, 38 p.

Barron, J.A., 1986a, Paleoceanographic and tectonic controls on deposition of the Monterey Formation and related siliceous rocks in California: Palaeogeography, Palaeoclimatology, Palaeoecology, v. 53, p. 27–45.

Barron, J.A., 1986b, Updated diatom biostratigraphy for the Monterey Formation of California, *in* Casey, R.E., and Barron, J.A., eds., Siliceous Microfossils and Microplankton of the Monterey Formation and Modern Analogs: SEPM, Pacific Section, Special Publication 45, p. 105–119.

Barron, J.A., and Isaacs, C.M., 2001, Updated chronostratigraphic framework for the California Miocene, *in* Rullkötter, J., and Isaacs, C.M., eds., The Monterey Formation: From Rocks to Molecules: New York, Columbia University Press, p. 393–395.

Barron, J.A., and Keller, G., 1983, Paleotemperature oscillations in the middle and late Miocene of the northeastern Pacific: Micropaleontology, v. 29, p. 150–181.

Behl, R.J., 1992, Chertification in the Monterey Formation of California and deep-sea sediments of the West Pacific [unpublished Ph.D. thesis]: University of California, Santa Cruz, 287 p.

Behl, R.J., 1999, Since Bramlette (1946): The Miocene Monterey Formation of California revisited, *in* Moores, E.M., Sloan, D., and Stout, D.L., eds., Classic Cordilleran Concepts: A View from California: Geological Society of America, Special Paper 338, p. 301–313.

Blake, G.H., 1981, Biostratigraphic relationship of Neogene benthic foraminifera from the southern California outer continental borderland to the Monterey Formation, *in* Garrison, R.E., and Douglas, R.G., eds., The Monterey Formation and Related Siliceous Rocks of California: SEPM, Pacific Section, Special Publication 15, p. 1–14.

Blake, G.H., 1994, Detailed biostratigraphy and paleoenvironmental interpretation of the Naples Bluff section, *in* Hornafius, J.S., ed., Field Guide to the Monterey Formation between Santa Barbara and Gaviota, California: American Association of Petroleum Geologists, Pacific Section, Field Guide, p. 17–28.

Burns, S.J., and Baker, P.A., 1987, A geochemical study of dolomite in the Monterey Formation, California: Journal of Sedimentary Petrology, v. 57, p. 128–139.

Bramlette, M.N., 1946, The Monterey Formation of California and the origin of its siliceous rocks: U.S. Geological Survey, Professional Paper 212, 57 p.

Chaika, C., and Williams, L.A., 2001, Density and mineralogy variations as a function of porosity in Miocene Monterey Formation oil and gas reservoirs in California: American Association of Petroleum Geologists, Bulletin, v. 85, p. 149–167.

Chang, A.S., and Grimm, K.A., 1999, Speckled beds: distinctive gravity-flow deposits in finely laminated diatomaceous sediments, Miocene Monterey Formation, California: Journal of Sedimentary Research, v. 69, p. 122–134.

De Kaenel, E., and Villa, G., 1996, Oligocene–Miocene calcareous nannofossil biostratigraphy and paleoecology from the Iberia abyssal plain, *in* Whitmarsh, R.B., Sawyer, D.S., Klaus, A., and Masson, D.G., eds., Proceedings of the Ocean Drilling Program, Scientific Results: v. 149, p. 79–145.

De Paolo, D.J., and Finger, K.L., 1991, High-resolution strontium-isotope stratigraphy and biostratigraphy of the Miocene Monterey Formation, central California: Geological Society of America, Bulletin, v. 103, p. 112–124.

Echols, R.J., 1994, Biostratigraphy of the Luisian and Mohnian stages between Santa Barbara and Gaviota, California, *in* Hornafius, J.S., ed., Field Guide to the Monterey Formation between Santa Barbara and Gaviota, California: American Association of Petroleum Geologists, Pacific Section, Field Guide, p. 29–44.

Espitalie, J., Deroo, G., and Marquis, F., 1985, La pyrolyse Rock-Eval et ses applications: Institut Français du Pétrole, Revue, v. 40, p. 563–579.

Ferrero, J., 1965, Dosage des principaux minéraux des roches par diffraction de Rayon X: Centre de la Formation en Pétrole (Bordeaux), Rapport, unpublished manuscript.

Ferrero, J., 1966, Nouvelle méthode empirique pour le dosage des minéraux par diffraction R.X.: Centre de la Formation en Pétrole (Bordeaux), Rapport, unpublished manuscript.

Filippelli, G.M., and Delaney, M.L., 1992, Similar phosphorus fluxes in ancient phosphorite deposits and a modern phosphogenic environment: Geology, v. 20, p. 709–712.

Filippelli, G.M., and Delaney, M.L., 1994, Phosphogenesis and the controls on phosphorus accumulation in continental margin sediments, *in* Iijima, A., Abed, A.M., and Garrison, R.E., eds., Siliceous, Phosphatic, and Glauconitic sediments of the Tertiary and Mesozoic: 29th International Geological Congress, Proceedings, Part C, p. 189–204.

Filippelli, G.M., Delaney, M.L., Garrison, R.E., Omarzai, S.K., and Behl, R.J., 1994, Phosphorus accumulation rates in a Miocene low oxygen basin: The Monterey Formation (Pismo Basin), California: Marine Geology, v. 116, p. 419–430.

Flower, B.P., and Kennett, J.P., 1993a, Relations between Monterey Formation deposition and middle Miocene global cooling: Naples Beach section, California: Geology, v. 21, p. 877–880.

Flower, B.P., and Kennett, J.P., 1993b, Middle Miocene Ocean Climate transition: High-resolution oxygen and carbon isotopic records from Deep Sea Drilling Project Site 588A, Southwest Pacific: Paleoceanography, v. 8, p. 811–843.

Flower, B.P., and Kennett, J.P., 1994a, Oxygen and carbon isotopic stratigraphy of the Monterey Formation at Naples Beach, California, *in* Hornafius, J.S., ed., Field Guide to the Monterey Formation Between Santa Barbara and Gaviota, California: American Association of Petroleum Geology, Pacific Section, Field Guide, p. 59–66.

Flower, B.P., and Kennett, J.P., 1994b, The middle Miocene climatic transition: East Antarctica ice sheet development, deep ocean circulation and global carbon cycling: Palaeogeography, Palaeoclimatology, Palaeoecology, v. 108, p. 537–555.

Föllmi, K.B., 1996, The phosphorus cycle, phosphogenesis and marine phosphate-rich deposits: Earth-Science Reviews, v. 40, p. 55–124.

Föllmi, K.B., and Garrison, R.E., 1991, Phosphatic sediments, ordinary or extraordinary deposits? The example of the Miocene Monterey Formation (California), *in* Müller, D.W., McKenzie, J.A., and Weissert, H., eds., Controversies in Modern Geology: London, Academic Press, p. 55–84

Föllmi, K.B., Garrison, R.E., and Grimm, K.A., 1991, Stratification in Phosphatic Sediments: Illustration from the Neogene of California, *in* Einsele, G., Ricken, W., and Seilacher, A., eds., Cycles and Events in Stratigraphy: Berlin, Springer-Verlag, p. 492–507.

Garrison, R.E., Hoppie, B.W., and Grimm, K.A., 1994, Phosphates and dolomites in coastal upwelling sediments of the Peru margin and the Monterey Formation (Naples Beach section), California, *in* Hornafius, J.S., ed., Field Guide to the Monterey Formation between Santa Barbara and Gaviota, California: American Association of Petroleum Geologists, Pacific Section, Field Guide, p. 67–84.

Garrison, R.E., Kastner, M., and Kolodny, Y., 1987, Phosphorites and phosphatic rocks in the Monterey Formation and related Miocene units, coastal California, *in* Ingersoll, R.V., and Ernst, W.G., eds., Cenozoic Basin Development in Coastal California: Rubey Volume 6: Englewood Cliffs, New Jersey, Prentice-Hall, p. 348–381.

Garrison, R.E., Kastner, M., and Reimers, C.E., 1990, Miocene phosphogenesis in California, *in* Burnett, W.C., and Riggs, S.R., eds., Phosphate Deposits of the World, vol. 3, Neogene to modern phosphorites: Cambridge, U.K., Cambridge University Press, p. 285–299.

Garrison, R.E., Kastner, M., and Zenger, D.H., Eds., 1984, Dolomites of the Monterey Formation and other organic-rich units: SEPM, Pacific Section, Special Publication 41, 215 p.

Gartner, S., 1992, Miocene nannofossil chronology in the North Atlantic, DSDP Site 608: Marine Micropaleontology, v. 18, p. 307–331.

Grimm, K.A., and Orange, D.L., 1997, Synsedimentary fracturing, fluid migration, and subaqueous mass wasting: intrastratal microfractured zones in laminated diatomaceous sediments, Miocene Monterey Formation, California, U.S.A.: Journal of Sedimentary Research, v. 67, p. 601–613.

Hilgen, F.J., Krijgsman, W., Raffi, I., Turco, E., and Zachariasse, W.J., 2000, Integrated stratigraphy and astronomical calibration of the Serravallian/Tortonian boundary section at Monte Gibliscemi (Sicily, Italy): Marine Micropaleontology, v. 38, p. 181–211.

Hodell, D.A., and Woodruff, F., 1994, Variations in the strontium isotopic ratio of seawater during the Miocene: Stratigraphic and geochemical implications: Paleoceanography, v. 9, p. 405–426.

Hornafius, J.S., 1991, Facies analysis of the Monterey Formation in the northern Santa Barbara channel: American Association of Petroleum Geologists, Bulletin, v. 75, p. 894–909.

Hornafius, J.S., 1994a, Overview of the stratigraphy of the Monterey Formation along the coastline between Santa Barbara and Gaviota, California, *in* Hornafius, J.S., ed., Field Guide to the Monterey Formation between Santa Barbara and Gaviota, California: American Association of Petroleum Geologists, Pacific Section, Field Guide, p. 1–15.

Hornafius, J.S., 1994b, Field trip road log to the Monterey Formation between Santa Barbara and Gaviota, California, *in* Hornafius, J.S., ed., Field Guide to the Monterey Formation between Santa Barbara and Gaviota, California: American Association of Petroleum Geologists, Pacific Section, Field Guide, p. 107–123.

Hornafius, J.S., 1994c, Correlation of volcanic ashes in the Monterey Formation between Naples Beach and Gaviota Beach, California, *in* Hornafius, J.S., ed., Field Guide to the Monterey Formation between Santa Barbara and Gaviota, California: American Association of Petroleum Geologists, Pacific Section, Field Guide, p. 107–123.

Ingle, J.C.J., 1980, Cenozoic paleobathymetry and depositional history of selected sequences within the southern California continental borderland, *in* Sliter, W., ed., Studies in Micropaleontology: Washington, D.C., Cushman Foundation for Foraminiferal Research, Special Publication 19, p. 163–195.

Isaacs, C.M., 1981, Lithostratigraphy of the Monterey Formation, Goleta to Point Conception, Santa Barbara coast, California, *in* Isaacs, C.M., ed., Guide to the Monterey Formation in

the California Coastal Area, Ventury to San Luis Obispo: American Association of Petroleum Geologists, Pacific Section, Special Publication 52, p. 9–24.
Isaacs, C.M., 1984, Hemipelagic deposits in a Miocene basin, California: Toward a model of lithologic variation and sequence, *in* Stow, D.A.V., and Piper, D.J.W., eds., Fine-Grained Sediments: Deep-Water Processes and Facies: Geological Society of London, Special Publication 4, p. 481–496.
Isaacs, C.M., 1985, Abundance versus rates of accumulation in fine-grained strata of the Miocene Santa Barbara basin, California: Geo-Marine Letters, v. 5, p. 25–30.
Isaacs, C.M., 2001, Depositional framework of the Monterey Formation, California, *in* Rullkötter, J., and Isaacs, C.M., eds., The Monterey Formation: From Rocks to Molecules: New York, Columbia University Press, p. 1–30.
Isaacs, C.M., and Peterson, N.F., 1987, Petroleum in the Miocene Monterey Formation, California, *in* Hein, J.R., ed., Siliceous Sedimentary Rock-Hosted Ores and Petroleum: Evolution of Ore Fields: New York, Van Nostrand Reinhold, p. 83–116.
Isaacs, C.M., Pisciotto, K.A., and Garrison, R.E., 1983, Facies and diagenesis of the Miocene Monterey Formation, California: A summary, *in* Iijima, A., Hein, J.R., and Siever, R., eds., Siliceous Deposits in the Pacific Region: Amsterdam, Elsevier, Developments in Sedimentology, v. 36, p. 247–282.
John, C., 1999, The Monterey Formation at El Capitan State Beach (Santa Barbara Basin, California) [unpublished diploma thesis]: University of Neuchâtel, 105 p.
Khan-Omarzai, S., Coe, R.S., and Barron, J.A., 1993, Magnetostratigraphy: a powerful tool for high-resolution age-dating and correlation in the Miocene Monterey Formation of California: results from Shell Beach section, Pismo Basin, *in* Aissaoui, D.M., McNeill, D.F., and Hurley, N.F., eds., Applications of Paleomagnetism to Sedimentary Geology: SEPM, Special Publication 49, p. 95–111.
Kennett, J.P., 1985, The Miocene Ocean: Geological Society of America, Memoir 163, 337 p.
Kleinpell, R.M., 1938, Miocene Stratigraphy of California: Tulsa, Oklahoma, American Association of Petroleum Geologists, 450 p.
Kleinpell, R.M., 1980, Miocene Stratigraphy of California Revisited: American Association of Petroleum Geologists, Studies in Geology, v. 11, 349 p.
Klug, H.P., and Alexander, L., 1974, X-ray Diffraction Procedures for Polycrystalline and Amorphous Materials: New York, John Wiley and Sons, 996 p.
Kolodny, Y., and Garrison, R.E., 1994, Sedimentation and diagenesis in paleo-upwelling zones of epeiric and basinal settings: a comparison of the Cretaceous Mishash Formation of Israel and the Miocene Monterey Formation of California, *in* Iijima, A., Abed, A.M., and Garrison, R.E., eds., Siliceous, Phosphatic, and Glauconitic Sediments of the Tertiary and Mesozoic: 29th International Geological Congress, Proceedings, Part C, p. 133–158.
Kübler, B., 1983, Dosage quantitatif des minéraux majeurs des roches sédimentaires par diffraction X: Institut de Géologie de Neuchâtel, Cahier, Série AX No. 1.1 & 1.2.
Kübler, B., 1987, Cristallinité de l'illite, méthodes normalisées de préparations, méthodes normalisées de mesures: Institut de Géologie de Neuchâtel, Cahier, Série ADX, p. 1–8.
MacKinnon, T.C., 1989, Petroleum geology of the Monterey Formation in the Santa Maria and Santa Barbara coastal and offshore areas, *in* MacKinnon, T.C., ed., Oil in the California Monterey Formation: 28th International Geological Congress, American Geophysical Union, FieldtripGuide Book T311, p. 11–27
Martini, E., 1971, Standard Tertiary and Quaternary calcareous nannoplankton zonation, *in* Farinacci, A., ed., Proceedings of the Second Planktonic Conference: Rome, Technoscienzia, p. 739–785.
Medrano, M.D., and Piper, D.Z., 1997, Fe–Ca–phosphate, Fe-silicate, and Mn-oxide minerals in concretions from the Monterey Formation: Chemical Geology, v. 138, p. 9–23.
Miller, K.G., and Feigenson, M.D., 1991, Miocene isotope reference section, Deep Sea Drilling Project site 608: An evaluation of isotope and biostratigraphic resolution: Paleoceanography, v. 6, p. 33–52.
Moore, D., and Reynolds, R., 1989, X-Ray Diffraction and the Identification and Analysis of Clay-Minerals: Oxford, U.K., Oxford University Press, 332 p.
Okada, H., and Bukry, D., 1980, Supplementary modification and introduction of code numbers to the low-latitude coccolith biostratigraphic zonation: Marine Micropalaeontology, v. 5, p. 321–325.
Pagani, M., Arthur, M.A., and Freeman, K.H., 1999, Miocene evolution of atmospheric carbon dioxide: Paleoceanography, v. 14, p. 273–292.
Pisciotto, K.A., and Garrison, R.E., 1981, Lithofacies and depositional environments of the Monterey Formation, California, *in* Garrison, R.E., and Douglas, R.G., eds., The Monterey Formation and Related Siliceous Rocks of California: SEPM, Pacific Section, Special Publication 15, p. 97–122.
Raymo, M.E., 1994, The Himalayas, organic carbon burial, and the climate in the Miocene: Paleoceanography, v. 9, p. 399–404.
Raymo, M.E., and Ruddiman, W.F., 1992, Tectonic forcing of late Cenozoic climate: Nature, v. 359, p. 117–122.
Raymo, M.E., Ruddiman, W.F., and Froelich, P.N., 1988, Influence of late Cenozoic mountain building on ocean geochemical cycles: Geology, v. 16, p. 649–653.
Reimers, C., Kastner, M., and Garrison, R.E., 1990, The role of bacterial mats in phosphate mineralization with particular reference to the Monterey Formation, *in* Burnett, W.C., and Riggs, S.R., eds., Phosphate Deposits of the World, vol. 3, Neogene to Modern Phosphorites: Cambridge, U.K., Cambridge University Press, p. 300–311.
Reimers, C., and Suess, E., 1983, Spatial and temporal patterns of organic matter accumulation on the Peru continental margin, *in* Thiede, J., and Suess, E., eds., Coastal Upwelling: Its Sediment Record, part B: New York, Plenum Press, p. 311–345.
Seilacher, A., 1969, Fault-graded beds interpreted as seismites: Sedimentology, v. 13, p. 155–159.
Stein, R., 1991, Accumulation of organic carbon in marine sediments: results from the Deep Sea Drilling Project/Ocean Drilling Program (DSDP/ODP): Berlin, Springer-Verlag, Lecture Notes in Earth Sciences, v. 34, 217 pp.
Summerhayes, C.P., 1981, Oceanographic controls on organic matter in the Miocene Monterey Formation, *in* Garrison, R.E., and Douglas, R.G., eds., The Monterey Formation and Related Siliceous Rocks of California: SEPM, Pacific Section, Special Publication 15, p. 213–219.
Vincent, E., and Berger, W.H., 1985, Carbon dioxide and polar cooling in the Miocene: The Monterey hypothesis, *in* Sundquist, E.T., and Broecker, W.S., ed., The Carbon Cycle and Atmospheric CO_2, Natural Variations Archean to Present: American Geophysical Union, Geophysical Monographs, v. 32, p. 455–468.
White, L.D., 1992, Overview of the Monterey Formation, dating techniques, sedimentary components, and paleoceanographic parameters, *in* Schwalbach, J.R., and Bohacs, K.M., eds., Sequence Stratigraphy in Fine-Grained Rocks: Examples from the Monterey Formation: SEPM, Pacific Section, Special Publication 70, p. 3–5.
White, L.D., Garrison, R.E., and Barron, J.A., 1992, Miocene intensification of upwelling along the California margin as recorded in siliceous facies of the Monterey Formation and offshore DSDP sites, *in* Summerhayes, C.P., Prell, P., and Emeis, K.C., eds., Upwelling Systems: Evolution since the Early Miocene: Geological Society of London, Special Publication 63, p. 429–442.

APPENDIX 1

Early Miocene (Burdigalian): Zone NN4

The interval between samples Cap 1 and Cap 23 belongs to Zone NN4 (Fig. 6, Table 2) on the basis of on the very rare occurrence of *Discoaster variabilis* at Cap 9 (estimated age of 17.74 Ma), the rare occurrence of *Calcidiscus premacintyrei* at Cap 20 (estimated age of 17.55 Ma) and a few occurrences of *Helicosphaera ampliaperta* at Cap 23. The top of the Burdigalian is approximated by the increase in abundance in *Helicosphaera ampliaperta* (estimated age of 16.48 Ma). The LO of *Discoaster deflandrei* observed at Cap 30 is placed just above the Burdigalian–Langhian boundary, and the few occurrences of *Helicosphaera ampliaperta* at CAP 23 can be used to define the top of the Burdigalian. The FO of *Calcidiscus premacintyrei*, a NN4 biohorizon, is observed at Cap 20.

Middle Miocene (Langhian): Uppermost Part of Zone NN4 to Lowermost Part of Zone NN5

The interval from CAP 26 to CAP 40 is Langhian in age. It includes the uppermost part of Zone NN4 and the lowermost part of Zone NN5. Several bioevents are recorded during this period: Sample CAP 26 yields the LO of *Sphenolithus heteromorphus.* This biohorizon corresponds to the base of the paracme in *Sphenolithus heteromorphus* dated at 16.40 Ma. Sample Cap 30 yields the LCO of *Discoaster deflandrei.* This biohorizon has an estimated age of 16.27 Ma and is used to place the NN4–NN5 boundary between samples Cap 30 and Cap 33.

Middle Miocene (Serravallian): Lower Part of Zone NN5 to Upper Part of Zone NN8

The interval between samples Cap 33 and Cap 105 belongs to Zone NN5. The Langhian–Serravallian boundary is placed between samples Cap 40 and Cap 44 by the FOs at sample level Cap 44 of *Discoaster exilis, Discoaster musicus, Discoaster petaliformis* and *Discoaster sanmiguelensis.* An age of 15.07 Ma is estimated for this biohorizon on the basis of the FO of *Discoaster petaliformis* (with birefringent central knob in Cap 44).

Instead of using the zonal marker *Sphenolithus heteromorphus* to place the NN5–NN6 boundary, we used the shift in dominance between *Cyclicargolithus floridanus* and *Reticulofenestra pseudoumbilicus* (forms larger than 8.0 microns). This bioevent corresponds to the LO of *Sphenolithus heteromorphus* and occurs at 13.52 Ma. It is situated between samples Cap 105 and Cap 108.

The interval between samples Cap 118 and Cap 134 belongs to Zone NN6. Sample Cap 131 yields the LO of *Discoaster petaliformis* (estimated age of 13.31 Ma). The FO of *Triquetrorhabdulus rugosus* (estimated age of 13.04 Ma) and the FO of *Calcidiscus premacintyrei* is observed in sample Cap 133. Sample Cap 134 contains the LOs of *Cyclicargolithus floridanus* and *Discoaster musicus.* The first bioevent is interpreted as a last consistent occurrence (LCO) and has an estimated age of 12.70 Ma. Also recorded at Cap 134 is the LO of elliptical forms of *Coronocyclus nitescens.* An estimated age of 12.42 Ma is obtained for this biohorizon (average of 12.70 and 12.14 Ma, LCO of *Cyclicargolithus floridanus*).

The NN6–NN7 boundary is identified by the FO of the zonal marker *Discoaster kugleri.* This species is recorded from sample Cap 143 onward, as is the FO of *Calcidiscus macintyrei* (forms larger than 11.0 microns) and the LO of *Discoaster sanmiguelensis.* The NN6–NN7 boundary lies between samples Cap 134 and Cap 143. Sample Cap 143 is the first sample analyzed for calcareous nannofossils above the first set of hardgrounds and has an estimated age of 11.67 Ma. This age is the

average of 11.83 Ma (FO of *Discoaster kugleri*) and 11.52 Ma (LO of *Discoaster kugleri*).

The interval between samples Cap 143 and Cap 145 belongs to Zone NN7. The LO of *Coccolithus miopelagicus* at Cap 145 is used to place the NN7–NN8 boundary. Also recorded at Cap 145 is a form transitional between *Discoaster micros* and *Catinaster coalitus.* Backman and Raffi (1997) recorded this transitional form and indicated that it occurred only from 10.820 to 10.790 Ma by calibration of their section with orbitally tuned time control. This allows us to give a very precise estimated age of 10.805 Ma (mean value) to sample Cap 145, which is situated just above the top of the condensed unit.

The FO of *Discoaster brouweri* at sample level CAP 151 indicates that the top of the measured El Capitan State Beach section is still in NN8. This sample has an age estimate of 10.69 Ma. Sample Cap 151 is situated about 13 meters above the top of the hardground intervals. At the nearby Naples Beach section, upper Miocene sediments were recorded at about 12 meters above the top of the condensed interval. The top sample of the Naples Beach section at 150.40 meters contains *Discoaster pentaradiatus, Discoaster pseudovariabilis, Minylitha convallis* and *Discoaster* aff. *D. bollii* (Badertscher 2000). The estimated age of 9.3 Ma obtained for this sample is used as top point to control the sedimentation accumulation curve of the El Capitan State Beach section.